SMASIS2008-539

EFFECTS OF BRAID ANGLE ON PNEUMATIC
ARTIFICIAL MUSCLE ACTUATOR PERFORMANCE

Michael F. Gentry   **Norman M. Wereley**
Department of Aerospace Engineering
University of Maryland
College Park, Maryland 20742

ABSTRACT

Pneumatic artificial muscles (PAMs) provide numerous advantages for use as actuators in a wide variety of mechanical systems. Our study focused on determining the effects of braid angle on the performance of PAMs. This paper discusses how we constructed a set of PAMs with varying braid angle, predicted their performance using analytical models, gathered empirical data characterizing the PAMs, and compared the analytical predictions with the experimental results. We constructed six PAMs of different braid angles between 38° and 73°. To predict PAM performance, we used an analysis based on the force equilibrium equations for a pressurized actuator. We first quantified the performance limits of each actuator in a series of static characterization tests. Then we subjected each PAM to cyclical displacement testing. Finally, a series of cyclical tests were performed with a pre-strain applied to the PAMs, to better approximate their typical use. Our results showed variation of braid angle causes significant differences in performance among the six PAMs tested; PAMs with larger braid angle generated higher blocked force and exhibited greater contraction. The empirical data matched the model predictions based on our estimates for the braid angle of a given PAM.

KEY WORDS: pneumatic artificial muscles, McKibben muscles, actuators

INTRODUCTION

Pneumatic artificial muscles are a type of pneumatic actuator that generate tensile force in the axial direction. The energy for this force generation comes from the pressure difference between the high-pressure gas inside and the ambient air outside the PAM. PAMs have an inner bladder which expands when inflated, and is harnessed within an outer woven sleeve. The sleeve consists of individual fibers woven into a cylindrical braid. As the inner bladder expands radially, it pushes on the relatively stiff fibers which in turn transfer the force along the longitudinal axis to the two ends. Through this process the PAM produces tensile force (if its ends are restrained) or contraction (if the ends are allowed to move freely). Several names exist in the literature for actuators which use inflated membranes to replicate the characteristics of biological muscles (e.g. fluidic muscle [1], pneumatic muscle actuator [2,3], McKibben artificial muscle [4,5,6], Rubbertuator [7,8], flexible matrix composite [9]); Daerden and Lefeber [10] present a comprehensive overview of their various properties.

PAMs were first developed by J. L. McKibben during the 1950's for use in orthotic systems [11] and were patented in 1958 by R. Gaylord as fluid actuated stroking devices [12]. They are increasingly being considered for use in a variety of applications, including powered prosthetics [13,14], robotic actuation [4,15,16], and aircraft flight control [17-19]. PAMs have a number of advantages as actuators, including:

- High force-to-weight and work-to-weight ratio
- Readily available, inexpensive, and lightweight working fluid (i.e. air)
- Low cost, robust components
- No risk of explosion or fire compared to hydraulics
- Ability to generate higher force output than conventional pneumatic cylinders at equivalent pressure [1]

The performance characteristics of PAMs depend on a number of factors, such as the dimensions and materials of the rubber hose and the plastic braid. This study focused on the effects of the braid angle θ_o, defined as the angle between any fiber of the outer woven braid and the radial axis, as seen in Fig. 1. The braid angle has been shown by Davis and Caldwell [2] to

Copyright © 2008 by ASME

affect the free contraction (i.e. pressurized but unconstrained) length and hysteretical behavior (through friction with the inner bladder), for PAMs whose contraction was limited by an inner bladder small enough to allow adjacent fibers of the braid to contact each other during free contraction. Our investigation studied these and other effects of braid angle on PAMs designed to produce larger forces, which necessitated
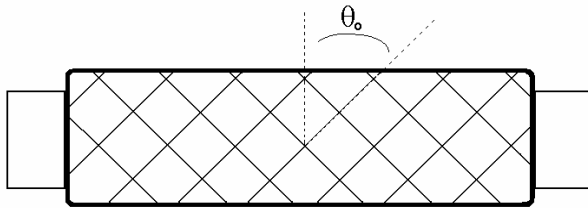

Figure 1. Definition of braid angle, θ_o.

larger diameter inner bladders. We determined that the most effective way to study the effects of a variety of braid angles was to construct several PAMs of the same inner bladder and different braid sleeve diameters; six PAMs were constructed with braid angles between 38° and 73°.

The performance limits of each actuator were quantified with the minimum contraction ratio, λ_{min}, and blocked force, F_b. The first is a metric of the stroke achieved by an unconstrained PAM at operating pressure; the second is defined as the force generated by a PAM fixed at its unpressurized length and inflated to operating pressure. These two bounds were sufficient for consideration of static performance and comparison with the analytical model used [5], but further testing was needed to explore dynamic effects over the range of stroke. To this end, we performed a series of cyclical loading tests and recorded position and force data throughout the cycle of each PAM's movement.

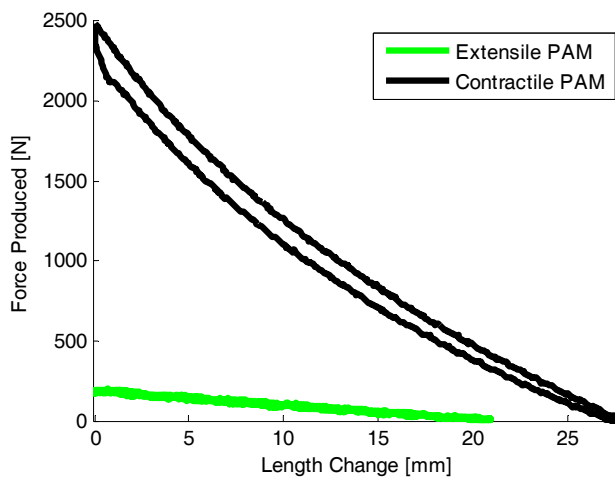It is worth noting that PAMs can be configured to extend

Figure 2. Force generated by extensile and contractile PAMs, over respective stroke.

rather than contract upon inflation. This is entirely dependent on the braid angle of the PAM. If the fibers of the braid cross at an angle less than about 36°, the radial expansion of the inner bladder will be transferred into axial extension and the PAM will generate compressive force at its ends. Figure 2 compares two of our PAMs, with braid angles of 72° (contractile) and 24° (extensile). The contractile PAM generates over 13 times the absolute value blocked force and about 34% larger stroke than the extensile PAM. Due to their relatively high force and large stroke, contractile PAMs are more feasible as actuators and as such remain the focus of our study.

Since PAMs configured in this way can only generate tensile force, they are often deployed in an antagonistic setup: two acting on opposite sides of a pulley, similar to the configuration of the triceps and biceps muscles controlling movement of the upper arm and elbow. In this and other situations, the PAM would experience an axial strain before it pressurized. We subjected our PAMs to a second round of cyclical loading tests under initial tension to determine the effect of this strain.

This paper describes our procedures for PAM fabrication, predictions of their performance, results from various tests, and finally a comparison of the empirical data with the analytical predictions.

CONSTRUCTION

All six PAMs made for this study were fabricated in-house. Their main components were a length of latex rubber hose, plastic braid woven into a tube, and short aluminum rods to cap either end. For the purpose of varying the angle of the plastic braid, the PAMs were constructed with different sized braids. The nominal sizes of the braid were listed by the manufacturer (Techflex, Inc. of Sparta, NJ) did not refer to either the minimum or maximum diameter, but they did reflect the braids' size relative to each other and as such we used them as labels to differentiate the PAMs throughout this study. We used ⅝ in., ¾ in., 1 in., 1 ¼ in., 1 ½ in., and 1 ¾ in. braids comprised of polyethylene terepthalate (PET) fibers. The sections of braid were wrapped around 100 mm (3.65 in.) long sections of 25.4 mm (1 in.) outer diameter rubber hose, as seen in Fig. 3.

With the hose and braid assembled, 25.4 mm (1 in.) long

Figure 3. Section of ⅝ in. Braid set over 25.4 mm (1 in.) tube. PAMs with smaller diameter braids had smaller braid angles.

2   Copyright © 2008 by ASME

sections of threaded rod were inserted into the rubber hose and secured inside of the hose and braid by steel wire wrapping. These two end fittings enclosed the volume of air within the PAM, and channeled the axial forces from the braid into the surrounding mechanical system. On one end, a hole drilled through the central axis of the entire end fitting allowed air flow in and out of the PAM.

At this time we noted a problem with some PAMs having a slight curvature due to the physical properties of the rubber hose. The tubing we use comes in coils from the manufacturer so any section cut from it has an inherent curve, as can be seen in each of the actuators in Fig. 4. We attempted to straighten the sections of tube, by tensioning them for several days, applying heat, forcing them to coil in the opposite direction, and various combinations thereof. These methods led to slight improvements, but some PAMs remained visibly curved. We continued to use these PAMs because the effects of curvature were eliminated once the PAM was pressurized or tensioned; that is, their typical use was unaffected.

Figure 4. From left to right, PAMs with braid angles of 40.9°, 38.10°, 58.57°, 60.51°, and 67.36°.

MODEL PREDICTION

To predict the effects of θ_o on the performance parameters F_b and λ_{min}, we used an analytical model based on force equilibrium equations over the entire PAM. Accurate predictions required knowledge of each PAM's θ_o, which was determined via the methods described below.

Analytical Model

To predict PAM performance, mathematical models have been derived from considerations such as volume change [20], force balancing [21], and finite element modeling [3,22]. These models are of limited accuracy due to the complex physical process they simulate, so further studies have proposed improvements to account for elastic energy storage in the bladder [6], curvature at the ends during inflation [23], and stress in the braid fibers [24]. The analytical model we used was built upon these existing models by Kothera, et al.

[5]. It uses force equilibrium equations for a pressurized PAM, with additions to compensate for non-uniform thickness throughout the hose and non-cylindrical shape near each end. The force F is found by inputting into Eqn. 1 the parameters pressure P, number of fiber turns N, reduced length L', bladder volume V_b, bladder thickness t, bladder radius R, bladder elastic modulus E_R, and the resting actuator length L_o.

$$F = \frac{P}{4N^2\pi}\left(3(L')^2 - B^2\right) + P\left(\frac{V_b}{L'} - \frac{t}{2\pi RN^2}(L')^2\right) +$$
$$E_R V_b\left(\frac{1}{L_o} - \frac{1}{L'}\right) + \frac{E_R L}{2\pi RN^2}\left(tL' - t_o L_o\right) \quad (1)$$

With L' referring to the length of the cylindrical section of the inflated PAM, related to its current length L and initial radius R_o in Eqn. 2.

The model predicts static response only, and quantifies the

$$L' = L - 2(R - R_o) \quad (2)$$

response with the characteristic parameters F_b and λ_{min}.

Measuring Braid Angle

The model was dependent on the braid angle, and this angle could only be measured after the PAM was fully assembled. The pliable and shifting nature of the braid adds a degree of ambiguity to geometrical measurement.

We used two different methods to determine the braid angle. The first method used the geometrical considerations, as shown in Fig. 5, which are referenced directly in the analytical model. For a PAM with length L and inner radius R_i, B is the length of a single braid fiber wound around and N is the number of turns that
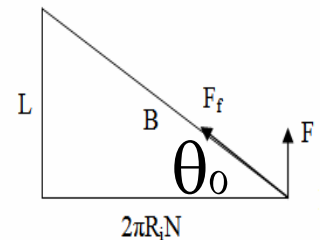
Figure 5. Geometry for calculating braid angle.

fiber makes around the diameter. By measuring L, R_i, B, and N trigonometric relations defined in Eqn. 3 below to solve for θ_o. However, the effectiveness of this geometric method was limited because the physical properties of the rubber hose and plastic braid prevented the PAMs from forming ideal cylinders.

$$\theta_o = \sin^{-1}(\frac{L}{B}) = \cos^{-1}(\frac{2\pi R_i N}{B}) \quad (3)$$

The second method more directly measured the angle. We began by rubbing a pencil over an area of the braid, about 25 mm (1 in.) square. Next, a piece of transparent tape was flattened over this area and carefully removed, bringing up with it a rubbing of the braid pattern. This tape was laid down on

3   Copyright © 2008 by ASME

white paper, and the braid angle was measured between patterns made by the pencil rubbings.

Visual inspection indicated that θ_o varies at different points around the circumference, caused by the curvature of the tube and slight inconsistencies in the construction process. Since the rubbing method only finds the braid angle of a small area, we took measurements from four points around the circumference of the actuator to obtain an average value of θ_o. We found that the braid angle measured from the four different sites on each PAM varied considerably, as seen in Table 1 below.

Predictions of Performance

The model is highly sensitive to variations in braid angle, as evidenced by the preliminary predictions of blocked force in Table 1. Although θ_o varied around the PAM, the mean of these four measurements was chosen as an estimate of the overall θ_o. The angle measured at locations corresponding to the interior and exterior of the hose-induced curvature were the smallest and largest (respectively) of the four angles measured, and the average between those two tended to be within 5% of the measured values of the two locations along the axis of curvature. Thus we took the mean of the angles from these four points to be an accurate approximation of the resting θ_o, unaffected by curvature.

Table 1. Estimates of braid angle.

Braid Size	θ_o Average	θ_o Range	F_b Variance
⅝ in.	40.09°	8.65°	502%
¾ in.	38.10°	4.61°	247%
1 in.	58.57°	8.62°	221%
1 ¼ in.	60.51°	3.85°	143%
1 ½ in.	67.36°	9.2°	269%
1 ¾ in.	72.40°	6.43°	225%

Table 1 shows the mean θ_o measured for each PAM, using the four-point direct-measurement method. The middle column lists the range in θ_o measured over each PAM, and to the right is the percent variance of predicted F_b over this

range. For example, the 1 in. braid PAM has θ_o measured between 53.5° and 62.1°. The model predicts a blocked force of 154 lb and 340 lb respectively, a 221% increase from one to the other.

TESTING

Each PAM was subjected to a series of tests to determine the effects of braid angle. We quantified the performance limits of each actuator by determining its minimum contraction ratio and blocked force.

Contraction ratio λ is defined with active length L_a as the resting length of the inflatable section (i.e. distance between the end fittings) and ΔL as the change in this length due to pressurization, as seen in Eqn. 4.

$$\lambda = \frac{L_a - \Delta L}{L_a} \qquad (4)$$

Static Characterization

To find values for λ, the active length of an unconstrained PAM was measured as pressure was applied from 0-621 kPa (90 psi) at 69 kPa (10 psi) intervals. This range of pressure represents the standard operating range for these actuators. λ_{min} occurs at the highest pressure, when the actuator is at its shortest length.

To find blocked force, we began by connecting the PAM in a fixed position to a servohydraulic material testing machine (MTS Systems Co., Model 64710A). The pressure was then increased from 0-621 kPa (90 psi) at 69 kPa (10 psi) intervals, and we recorded the axial force measured by the machine at each of these increments.

During the testing, there were immediately noticeable differences between the different braid angle actuators. In free contraction testing, actuators with larger braid angles (58.57°, 60.51°, 67.36°, and 72.4°) became markedly shorter and wider than those with smaller θ_o.

Table 2 compares the free contraction of two of the PAMs. Each is shown with no pressure and pressurized to 621kPa (90psi). On the right, the change in length of the actuator with θ_o

Table 2. Free contraction of large and small braid angle PAMs.

	$\theta_o = 67.36°$	$\theta_o = 40.09°$
0 kPa (0psi)		
621 kPa (90psi)		

Copyright © 2008 by ASME

= 40.09° is nearly imperceptible, whereas on the right the θ_o = 67.36° actuator shows a significant decrease in length and increase in diameter.

Figure 6 shows the F_b and λ_{min} for the PAMs in this study, as denoted by the points along the right and bottom axes,
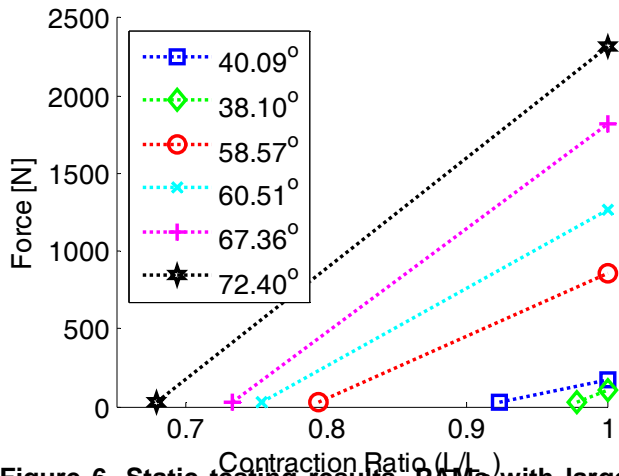

Figure 6. Static testing results. PAMs with larger θ_o had greater F_b and smaller λ_{min}.

respectively. The line connecting each pair of values is a linear approximation of each actuator's load line. The linearized load lines provide an estimate of PAM performance, in terms of contraction ratio and force, when pressurized at 621kPa (90psi).

Among the oversized braids (i.e. larger braid diameter than inner bladder diameter), performance drops with smaller diameter whereas the two undersized braids exhibit an opposite trend. As noted previously, the nominal diameters of the braid were only useful in naming the PAMs. In the case of the two undersized PAMs, the actuator made with ¾ in. braid has a smaller braid angle (see Table 1) than the ⅝ in. PAM. This discrepancy explains why the ⅝ in. PAM had more stroke and force than the ¾ in., though an intuitive prediction based on the braid diameter would have expected otherwise.

Quasi-Static Cyclical Loading

In order to learn more about PAM response over the entire cycle, each actuator was tested on the MTS machine programmed to record data continuously. The program consisted of a steady displacement ramp from initial length (blocked force) to each PAM's free contraction length (zero force), a ten-second hold at that displacement, then another displacement ramp back up to the original length. The actuators were pressurized to 621kPa (90psi) for the duration of the test. The results can be seen in Fig. 7.

Similar to Figure 6, the data in Figure 7 indicate that the PAMs made with larger braids (corresponding to larger θ_o) have higher blocked force and lower minimum free contraction ratio. Figure 7 also shows the effects of hysteresis, which is evident to some extent in all the PAMs and most

significant in those with larger braid angles. The hysteresis loops are all clockwise, as the PAMs produced more force as they were being stretched from $\lambda = \lambda_{min}$ to $\lambda = 1$. The hysteretical
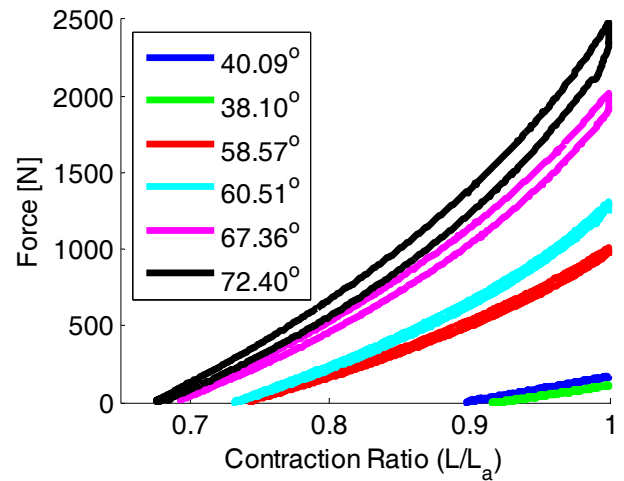

Figure 7. Cyclical loading results. Nonlinear effects of hysteresis were more profound in PAMs with large θ_o.

trends exhibited by the data suggest that the linearized load lines in Figure 6 are not accurate estimates of clearly nonlinear PAM behavior.

Cyclical Loading with Pretension

To further define the performance of these PAMs, they were tested for a second time in the MTS machine under cyclical loading conditions, with the machine reprogrammed to pull the PAMs to 105% of their total length before allowing them to contract to their λ_{min}.

When the pressurized PAMs were tensioned above $\lambda = 1$, the rate at which they generated force increased, as seen in Fig. 8.
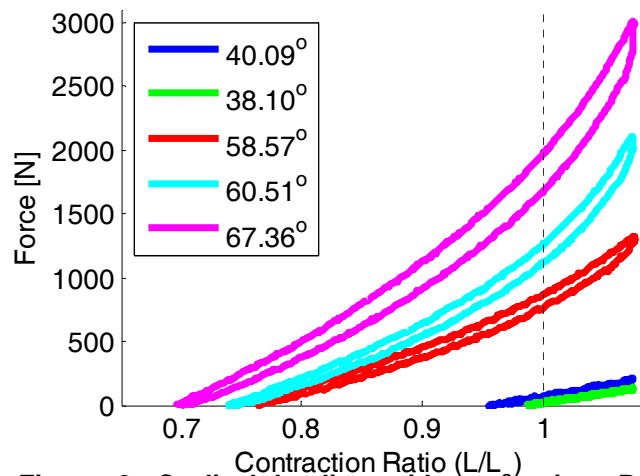

Figure 8. Cyclical loading with pretension. PAMs with larger θ_o stiffened quicker as they were

5   Copyright © 2008 by ASME

This was caused by the stiffening of the plastic braid under tension. This effect was more pronounced in the PAMs with larger braids and θ_o, as the braid fibers in these PAMs were initially closer to being aligned with the longitudinal axis.

COMPARISON BETWEEN MODEL AND EXPERIMENT

Figure 9 shows the experimental results for F_b (top) and λ_{min} (bottom) for each PAM, as a function of their resting braid angle. The horizontal bars represent the maximum range in measured braid angle, with the central square at the average of this measured range (see Table 1). The minimum free contraction ratio linearly decreases as the braid angle increases, while the trend for the maximum force is approximately an increasing polynomial function of braid angle. These observations are matched by the model
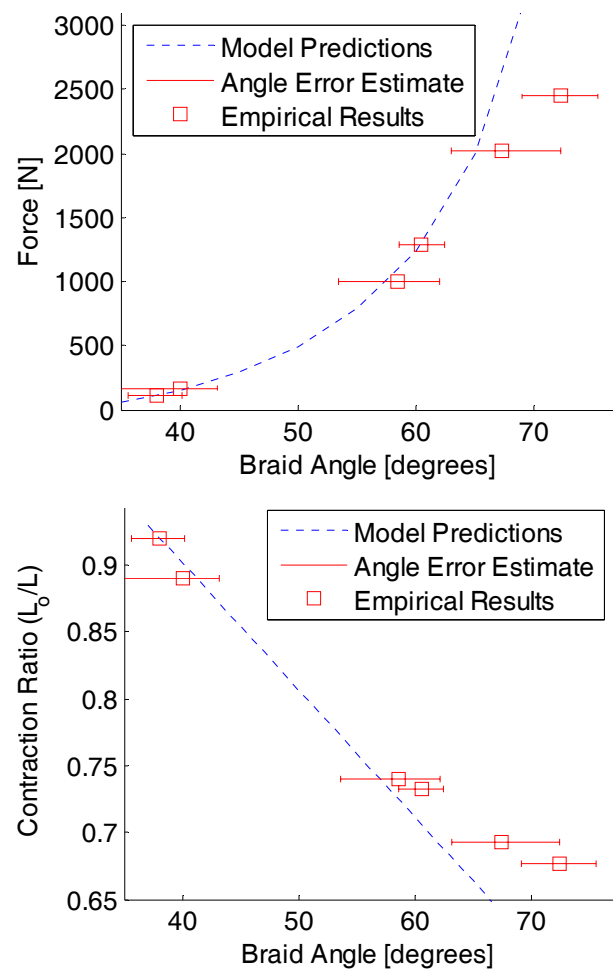

Figure 9. F_b **(top) and** λ_{min} **(bottom) as function of braid angle. Dashed curves are predictions from the analytical model; horizontal bars denote range of measured braid angle.**

predictions, shown in Fig. 9 with the dashed curves.

The model force predictions are close to the experimental data for the 40.9^O, 38.10^O, 58.57^O, and 60.51^O PAM. The predictions for the 67.36^O PAM are within the range of its measured braid angle. However, the model clearly is less accurate for the larger values of braid angle, which is also the case for the predictions of minimum contraction.

CONCLUSION

Pneumatic artificial muscles offer positive benefits for use in a range of mechanical systems. Their general performance characteristics have been documented, and their behavior predicted with analytical and numerical models.

Our main goals were to experimentally determine what effects the braid angle has on the performance of a PAM, and to try to predict these effects accurately with an analytical model. The data show that variation of the braid angle has a dramatic effect on the minimum free contraction ratio and the maximum blocked force. An increase in the braid angle significantly increases the stroke of the actuator, as well as causing more force to be produced at any value of λ, with no significant increase in weight, fabrication complexity, or cost.

The analytical model was fairly accurate in predicting the performance of most of the PAMs, but was less accurate for the larger values of θ_o. This could be due to the greater slack between the braid and the uninflated bladder in the larger PAMs, or as yet unaccounted-for interactions between the braid fibers and the inflated bladder.

REFERENCES

[1] Lightned, S., and Lincoln, R., 2002, "The Fluidic Mucle: A 'New' Development," International Journal of Modern Engineering, **2**(2).
[2] Davis, S., and Caldwell, D, 2006, "Braid Effets on Contractile Range and Friction Modeling in Pneumatic Muscle Actuators," International Journal of Robotics Research, **25**(4), pp. 359-369.
[3] Zhou, B., and Accorsi, M., 2004, "A New Finite Element for Modeling Pneumatic Muscle Actuators," Computers & Structures, **82**(11-12), pp. 845-846.
[4] Tondu, B., and Lopez, P., 1997, "The McKibben Muscle and its Use in Actuating Robot-arms Showing Similarities with Human Arm Behaviour," Industrial Robot, **24**(6), pp. 432.
[5] Kothera, C., et al., 2006, "Experimental Characterization and Static Modeling of McKibben Actuators," Proc. ASME International Mechanical Engineering Congress and Exposition, Chicago, IL.
[6] Klute, G., and Hannaford, B., 2000, "Accounting for Elastic Energy Storage in McKibben Artificial Muscle Actuators," Journal of Dynamic Systems, Measurement, and Control, **122**(2), pp. 386-388.
[7] Van der Smagt, P., Groen, F., and Schulten, K., 1996, "Analysis and Control of a Rubbertuator Arm," Biological Cybernetics, **75**, pp. 433-440.

[8] Ozkan, M., et al., 2000, "Defining a Neural Network Controller Structure for a Rubbertuator Robot," Neural Networks, **13**(4-5), pp. 533-544.

[9] Shan, Y., et al., 2006, "Nonlinear-elastic Finite Axisymmetric Deformation of Flexible Matrix Composite Membranes Under Internal Pressure and Axial Force," Composites Science and Technology, **66**, pp. 3053–3063.

[10] Daerden, F., and Lefeber, D., 2002, "Pneumatic Artificial Muscles: Actuators for Robotics and Automation," European Journal of Mechanical and Environmental Engineering, **47**(1), pp. 10-21.

[11] Nickel, V., et al., 1965, "Synthetically Powered Orthotic Systems," Journal of Bone and Joint Surgery, **45A**(5).

[12] Gaylord, R., 1958. Fluid Actuated Motor System and Stroking Device. United States Patent No. 2,844,126.

[13] Ferris, D., et al., 2005, "An Ankle-Foot Orthosis Powered by Artificial Pneumatic Muscles," Journal of Applied Biomechanics, **21**(2), pp. 189–197.

[14] Vimieiro, C., et al., 2005, "Development of a Hip Orthosis Using Pneumatic Artificial Muscles," Proc. Technology Meets Surgery International, Sao Paolo, Brazil.

[15] Tondu, B., Ippolito, S., and Guiochet, J, 2005, "A Seven-Degrees-of-Freedom Robot-Arm Driven by Pneumatic Artificial Muscles for humanoid Robots," International Journal of Robotics Research, **24**(4), pp.257-274.

[16] Caldwell, D., Tsagarakis,N, et al., 2001, "A Pneumatic Muscle Actuator Driven Manipulator for Nuclear Waste Retrieval," Control Engineering Practice, **9**(1), pp.23-36.

[17] Woods, B., Bubert, E., Kothera, C., and Wereley, N., 2008, "Design and Testing of a Biologically Inspired Pneumatic Trailing Edge Flap System," Paper No. AIAA-2008-2046, Proc. AIAA Structures, Structural Dynamics, and Materials Conference, Schaumberg, IL.

[18] Kothera, C., Woods, B., Sirohi, J., Wereley, N., and Chen, P., Techno-Sciences, Inc., Beltsville, MD, U.S. Patent Application Pending for "Fluid-Driven Artificial Muscles as Mechanisms for Controlled Actuation," filed 11 Aug. 2006.

[19] Bubert, E., Woods, B., Kothera, C., and Wereley, N., 2008, "Design and Fabrication of a Passive High-Strain Morphing Aircraft Skin," Paper No. AIAA-2008-2045,Proc. AIAA Structures, Structural Dynamics, and Materials Conference, Schaumberg, IL.

[20] Chou, C., and Hannaford, B., 1996, "Measurement and Modeling of McKibben Pneumatic Artificial Muscles," IEEE Transactions on Robotics and Automation, **12**(1), pp. 90-102.

[21] Ferraresi, C., Franco, W., and Bertetto, A., 2001, "Flexible Pneumatic Actuators: A Comparison Between the McKibben and Straight Fibres Muscles," Journal of Robotics and Mechatronics, **13**(1), pp. 56–63.

[22] Ramasamy, R., et al., 2005, "An Application of Finite Element Modeling to Pneumatic Artificial Muscle," American Journal of Applied Science, **2**(11), pp. 1504-1508.

[23] Tsagarakis, N. and Caldwell, D, 2000, "Improved Modeling and Assessment of Pneumatic Muscle Actuators," Proc. IEEE International Conference on Robotics and Automation, San Francisco, CA.

[24] Davis, S., Tsagarakis, N. and Caldwell, D., 2003, "Enhanced Modelling and Performance in Braided Pneumatic Muscle Actuators," International Journal of Robotics Research, **22**(3-4), pp. (213-227).